Thermodynamics and Reduction Kinetics of Iron(III) Benzohydroxamic Acid Complex by Hydroxylamine Hydrochloride

[1]Muhammad Perviaz*, [2]Shazia Nisar, [2]Shazia Ishfaq, [2]Kanwal Zahid, [3]Muhammad Atif, [4]Fazal Rahim, [5]Ajmal Khan and [1]Zulkifle Ikram

[1]Department of Basic and Applied Sciences, Faculty of Science and Technology, University of Central Punjab, Lahore, Pakistan.

[2]Department of Chemistry, Faculty of Sciences, University of Karachi, 75270, Pakistan.

[3]Department of Chemistry, University of Education Lahore (Vehari Campus).

[4]Department of Chemistry, Hazara University, Mansehra, Pakistan.

[5]Natural and Medical Sciences Research Center, University of Nizwa, Oman Sultanate.

muhammad.perviaz@ucp.edu.pk*

(Received on 5th September 2023, accepted in revised form 5th August 2025)

Abstract: Using a stopped flow, the photodiode array spectrometer was employed to study the reduction kinetics of Iron(III)-Benzohydroxamic acid(BHA) complex with pH having 4.5 to 3 and temperature ranging from 298 K to 278 K. KCl was used to set the ionic strength of the system to 0.2 M. Pseudo first-order kinetics were studied to understand the reduction process. The rate constant was also calculated for 2nd order as well. It has been reported that in around 10 to 11 seconds more than half of Iron-BHA complex had been reduced while after around 120 seconds, the concentration of the complex was negligible as was completely reduced. For phase 1, the rate constant with pH 3 for temperature 278 K, 283 K, 288 K, 293 K and 298 K was 0.2120, 0.4310, 0.2900, 0.2770 and 0.5550 M^{-1} s^{-1} respectively. For pH 3.5 it is 0.1980, 0.2450, 0.3710, 0.5440 and 0.7150 M^{-1} s^{-1}. It was 6.5740, 6.5740, 9.8980, 13.1500 and 18.4800 M^{-1} s^{-1} for pH 4 and for pH 4.5 it was reported to be 6.5740, 9.8980, 21.0700, 20.3400 and 35.1600 M^{-1} s^{-1} respectively. For phase 2, at pH 3 it was reported to be 0.0990, 0.1290, 0.1690, 0.2120 and 0.2750 M^{-1} s^{-1} respectively. At pH 3.5 the rate constant was 0.0850, 0.1060, 0.1320, 0.1410 and 0.1790 M^{-1} s^{-1}. For pH 4, the rate was 6.5740, 6.5740, 17.1300, 25.1600 and 29.5100 M^{-1} s^{-1}, while it was 6.5740, 6.5740, 10.5500, 42.8000 and 39.3700 M^{-1} s^{-1} at pH 4.5 respectively. Thermodynamic parameters were then calculated such as Change in Enthalpy, entropy and activation energy. This study elucidates the thermodynamic and kinetic parameters governing the reduction of the Iron Benzohydroxamic Acid complex. The derived thermodynamic values and proposed kinetic mechanism contribute to a deeper understanding of iron coordination chemistry and redox processes relevant to various chemical and biological systems. These findings provide a foundation for future research exploring similar metal-ligand interactions.

Keywords: Photodiode, Kinetics, Pseudo first-order, Iron-BHA complex, Enthalpy, Entropy, Thermodynamic.

Introduction

Iron is an essential part of different biological and metabolic molecules like cytochromes and Fe-S proteins, as enzymes [1] during electron transportation. Iron mainly exists in two different forms such as Fe^{+2} and Fe^{+3}. The solubility of Fe(III) being only 10^{-18} M as compared to Fe(II) is the reason for its lower bioavailability than Fe(II) under physiological pH [2] .

Moreover, under aerobic conditions, Fe(II) undergoes oxidation and is converted to Fe(III) following Fenton's reaction. However, the Fenton reaction is non-favorable for biological organisms as free radicals are produced during the reaction [3]. The free radicals can disturb the nature of the surrounding tissue. Hence, a method of chelating the Fe(III) has been developed and when needed, converting the Fe(III) into Fe(II) using various biological reductants can be carried out. This will result in addressing the problem associated with the bioavailability of the both iron forms and also ensures the limitation of Fenton reaction pathway.

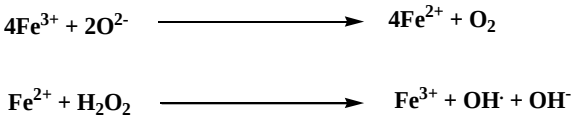

Scheme1: Fenton Reaction.

Various microorganisms and other living organisms have this mechanism to produce siderophores in order to chelate the iron molecules. Siderophore means "iron carrier", they are low molecular weight, mostly 600 Dalton and ranging from (200-2000) Dalton in size [4],

*To whom all correspondence should be addressed.

which bacteria, fungi and other microorganisms can produce. Siderophores are mostly water soluble with high binding constants [5; 6] and can be easily transferred to the environment. This property is unique and appears in the case of mycobactin for the production of mycobacteria [7]. Some microorganisms depend on the other microorganism for siderophores because they cannot produce it directly for their growth. As the iron is a crucial source of nutrient, and is limited in the environment, the microbes, using these siderophores outcompete the surrounding microorganisms and through efficient utilization and synthesis of siderophores, the microorganisms store [8; 9], and use iron based on their own needs gaining a competitive advantage over their surrounding competitor microorganisms for the limited iron in the environment [10-15]. Various major siderophore classes have been studied overtime and their formation constants are well reported [16].

The siderophore complexes having iron (III), usually have quite a negative redox potential, ranging in-between -750 mV and -350 mV (versus NHE) [17]. Consequently, using biological reducing agents such as reduced nicotinamide adenine dinucleotide phosphate (NADH or NAPH), -320 mV Vs NHE, to reduce siderophore complexes of Fe(III) becomes particularly challenging.

It has also been found tha the redox potential of Fe(III) siderophore complexes are greatly affected by the pH as the acidity or alkalinity of the environment results in the structural changes. The hydrogen atoms dissociate and result in deprotonation of the complex at acidic pH and consequently, the stable complexes break apart and various less stable complexes are formed. This results in the biological reductants to find it easier and more capable to donate electrons to the Fe(III) complexes now formed as the complexes become much more available to the reducing agents. This results in the shift in the redox potential of the system and changing it from extremely negative to rather positive values [18; 19; 20; 21]. This results in complexes that are rather prone to reduction. Hence, the need of developing good biological reductants arrives. In this study, biological reductants that can easily reduce Fe(III) complexes to Fe(II)-siderophore complex has been studied.

The Fe(III) complex formation constant value ($\log\beta$ = 30-50) [15; 22; 23; 24] illustrates a tendency for Fe(III) to be reduced into Fe(II) [18; 25; 26; 27; 28] by the usage of different biological reductants [29; 30; 31; 32]. Hydroxylamine hydrochloride has enough reducing ability [33] that correlates directly with the variations in pH. Reduction tendency increases with the formation of the complex at higher pH and smaller change appears as rate constant k_{obs} rises up. The redox potential of hydroxylamine hydrochloride is -0.387 V Hence, the study focuses on the reduction of Fe(III)BHA complex using hydroxylamine hydrochloride to Fe(II)-BHA complex.

This study aims to elucidate the mechanisms by which the two predominant oxidation states of iron—ferrous (Fe^{2+}) and ferric (Fe^{3+})—become bioavailable and influence biological systems under physiologically relevant pH conditions. Central to this investigation is the Fenton reaction, where redox cycling between Fe^{2+} and Fe^{3+} catalyzes the generation of hydroxyl radicals and other reactive oxygen species (ROS), leading to molecular and tissue-level oxidative damage [1,3,24]. To achieve this, the research incorporates chemical, microbiological, and biophysical approaches to understand iron-mediated oxidative stress and its mitigation. Key objectives include: (i) characterizing how microorganisms regulate siderophore production and secretion to scavenge iron in nutrient-poor environments [2,5,8]; (ii) quantifying the intrinsic redox potentials of representative Fe-siderophore complexes and their reducibility by biologically relevant reductants, using hydroxylamine hydrochloride as a model electron donor [10,14,25]; (iii) mapping the biosynthetic pathways, transport dynamics, and uptake mechanisms involved in siderophore-mediated iron acquisition [6,7,13]; (iv) assessing the effects of incremental pH changes on the redox potential and reduction susceptibility of Fe complexes [15,19]; (v) measuring the efficiency of hydroxylamine hydrochloride in reducing Fe-siderophore complexes to the more bioavailable Fe^{2+} form [12,28]; and (vi) synthesizing these insights to propose strategies for leveraging endogenous or exogenous reductants to suppress Fenton-driven ROS formation, thereby promoting safe iron utilization in cellular environments [18,25].

Experimental

pH Meter

HANNA pH Meter (Model HI83141) or JENWAY 430 were used throughout the experiments to measure the pH of the solutions. The pH meter was calibrated by standard buffer solution of pH 4.0, pH 7.0 and pH 10 before measurement of buffer solutions and other solutions.

HP 8452A Photodiode Array Spectrophotometer

The HP 8452A photodiode array spectrophotometer was used for kinetics studies of the reactions. This instrument was properly calibrated through different methods using manual.

a) Wavelength accuracy in scan mode.
b) Wavelength reproducibility in scan mode.
c) Wavelength reproducibility in rapid scanning mode.
d) Baseline test

Instrumentation

HP 8452A Photodiode Array Spectrophotometer

When the diode array spectrophotometer starts, it performs its internal calibration. The instrument wavelength is also calibrated by inserting a Holmium oxide filter into rectangular cuvette holder. The spectrum of the deuterium lamp is taken for the calibration of the wavelength, which has a multiple sharp peaks including a major emission peak at 656 nm. When the wavelength mis-calibrated the wavelength scale, it shows spikes in the spectrum. It needs a re-calibration of the instrument by standard method given in the instruction manual.

The HP 8452A diode array spectrometer (Fig 2.1) is a single beam, microprocessor controlled, UV-Visible spectrometer with collimating optics. It is faster than the conventional spectrophotometer with diode array technology. It has high sensitivity and precision and reproducible results than other conventional spectrophotometer.

The UV-Visible range of this instrument is 190 nm to 820 nm. Each diode covers a wavelength range of 2 nm.

Fig. 2.1: Diagram of Hewlett Packard 8452A diode array spectrophotometer.

Stopped-flow Mixing Accessory

The Applied photo physics RX-2000 stopped flow accessory (Fig 2.2) is compatible to photodiode array spectrophotometer having two path length 1cm and 0.2cm. The temperature of the reagent solutions were maintained by recirculating thermostatted water bath.

Fig. 2.2: Diagram of Photo-physics RX-2000 stopped flow accessory.

The equal volume of each reagent is mixed in observation chamber after pushing the both drive syringes simultaneously. The concentration of each reagent becomes half of its initial concentration in observation chamber.

The entire flow circuit including drive syringes is thermostatted, providing reliable temperature equilibration. The RX.2000 cell attaches in seconds without tools to any spectrometer that can accommodate a standard 1.0 cm rectangular cell. High performance syringes with canted seals provide reliable operation over a 0-60 ˚C temperature range. The drive syringes is changed to deliver mixing ratios from 1:1 to 1:25. The position of the stopping block/trigger mechanism can be adjusted to change the drive volume; important for large ratio asymmetric mixing experiments and purging air bubbles. The dead time is only 6 ms, making it possible to measure first order and pseudo first-order reaction rates over 200 s^{-1}.

Buffers Preparation:

The buffer solutions were prepared by dissolving 2 moles of formic acid in distilled water and combining it with 2 molar solution of Sodium Hydroxide (100 mL). Four buffer solutions having pH of 4.5, 4, 3.5 and 3 were produced by controlling the formic acid addition. This solution was diluted to around 2 liters using deionized water. The ionic strength was set to be around 0.2 M by employing various salts, ionic in nature. Buffer of acetate with a pH of 6, 5 and 4.5 was also produced in a similar manner.

Fe-BHA complex formation:

To prepare the complex of Fe-BHA, $Fe(NO_3)_3.9H_2O$ was used as the iron precursor. The precursor was dissolved in deionized water. The contents of the flask were then subjected to nitric acid which resulted in stopping of hydrolysis. The reaction mixture was shifted into a volumetric flask (250 mL) and water was added up to the mark. For the standardization of Iron, Iron-Opt method was employed. The analysis showed the concentration to be 5mM. The solution was further diluted and concentration was set to be 0.2 mM. $Fe(NO_3)_3.9H_2O$ (1.65 mL, 0.01 M) and 0.0274 g of BHA were added to a 250 mL volumetric flask and buffer solution of the desired pH was added as the solvent, having a specific ionic strength. At high pH, the solution appeared to be dull-red in color and when the pH ranged from 3.0-4.0±0.1, it appeared to be reddish orange.

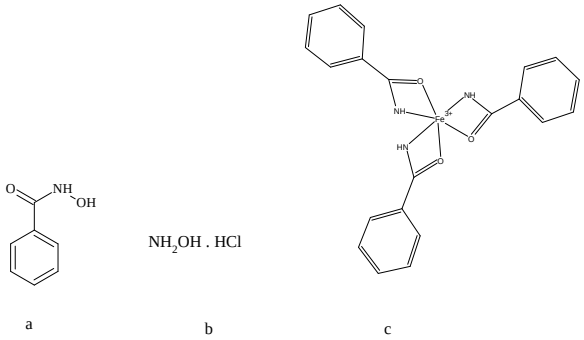

Fig. 1: Structure of: (a) Benzohydroxamic Acid (BHA); (b). Hydroxylamine Hydrochloride (NH_3OH^+ Cl^-); (c) Iron-Benzohydroxamic Acid complex [Fe(III)-BHA complex].

Preparation of Hydroxylamine Hydrochloride solution

A 25.485 mM solution of hydroxylamine hydrochloride was prepared by adding 0.8856 g in a 250 mL volumetric flask and adding distilled water up to the mark. Nitrogen gas was added to remove and cease any oxidation happening. Different solutions were then created using various buffers having different pH.

Kinetic Studies

An HP 8452A Photodiode array spectrophotometer was used to study the reduction kinetics of Iron BHA complex under pseudo-first order conditions, while hydroxylamine hydrochloride being used as reductant. The Photodiode array spectrophotometer was hyphenated with an RX-2000 stopped flow with path length of 0.2 cm and 1 cm. The wavelength of interest was 486 nm. The hydroxylamine hydrochloride was used to reduce 0.2 mM Fe(III)-BHA complex. The reductant concentration was around 7.5 mM to 15 mM. Temperature range was set to be 25 °C to 5 °C.

Results and Discussions

At 25±0.5 ºC, with a pH of 4.5±0.1, Fe(III)-BHA complex showed a sharp distinct peak with a lambda max of 486 nm. The ionic strength was set to be 0.2 M (KCl) while the concentration of Fe-BHA complex was 1.997×10^{-4} M. The UV-Visible spectrum can be observed in Fig 2. The molar absorptivity of the Fe(III)-BHA complex having different concentration at different pH can be observed in Table 1. It can be further observed in the kinetic studies that a significant portion of Fe(III)-BHA complex was reduced in just 10 seconds time, when exposed to Hydroxylamine hydrochloride. The concentration of Fe(III)-BHA complex was 1.997×10^{-4} M, Concentration of the reductant was set to be 1.019×10^{-2} M, the temperature was 15.0±0.5 °C, pH was set at 3.5±0.1 and the reaction was carried out having the ionic strength of the system to be 0.2 M maintained by KCl. It can be seen that with the passage of just a small time, a significant portion of Fe(III)-BHA has been reduced as the absorption is decreasing and around 120 second, most of the complex had already been reduced. The change in absorption and the reduction of Fe-BHA complex can be observed in Fig 3.

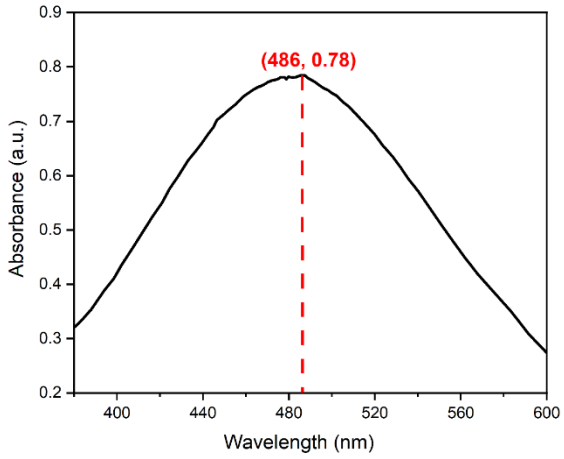

Fig. 2: Lambda Max of Fe(III)-BHA Complex.

Table-1: Molar Absorptivity of Iron-BHA complex at different pH having different concentration of BHA and Fe(III)-BHA complex.

pH	[Fe^{III}-BHA]	[BHA]	λ (nm)	Absorbance	Molar Absorptivity ($M^{-1}.cm^{-1}$)
3.0	**1.997×10^{-4} M**	**1.006×10^{-3} M**	**426**	**0.5875**	**2942**
3.5	**1.997×10^{-4} M**	**1.006×10^{-3} M**	**474**	**1.2851**	**6435**
4.0	**2.5×10^{-5} M**	**1.25×10^{-4} M**	**468**	**0.2355**	**4710**
4.5	**2.5×10^{-5} M**	**1.25×10^{-4} M**	**474**	**0.3041**	**6082**

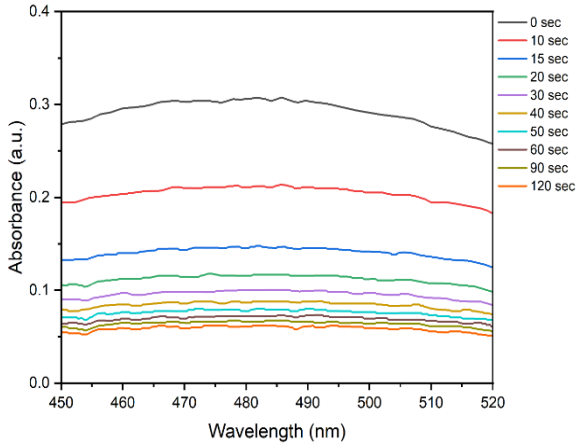

Fig. 3: Change in Fe(III)-BHA absorption over time.

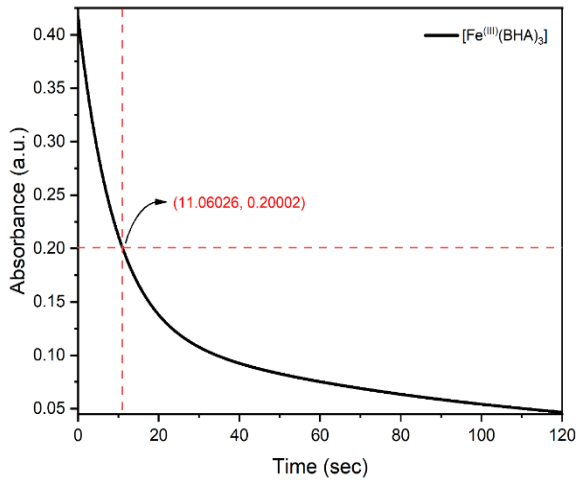

Fig. 4: Kinetic Spectrum of Reduction of Iron-BHA complex over time using Photodiode Array Spectroscopy.

Similarly, in Fig. 4 the same pattern can be observed and in just 11 seconds we can see almost half of the Fe(III)-BHA complex had been reduced. Because the reducing agent worked so quickly, the use of a stopped flow was necessary. It can be also be observed in Fig. 4 that the absorbance is 0.200 at the 11 second mark which is an indication that the absorbance has halved and half of the concentration of Fe(III)- BHA complex has already been reduced. Also, the change in absorbance over time and the kinetic spectrum shows that reaching 120 seconds, almost negligible to no amounts of Fe(III)-BHA complex remained in the system as it all got reduced. The 3D kinetic spectrum of reduction of Fe(III)-BHA can also be observed in Fig 5.

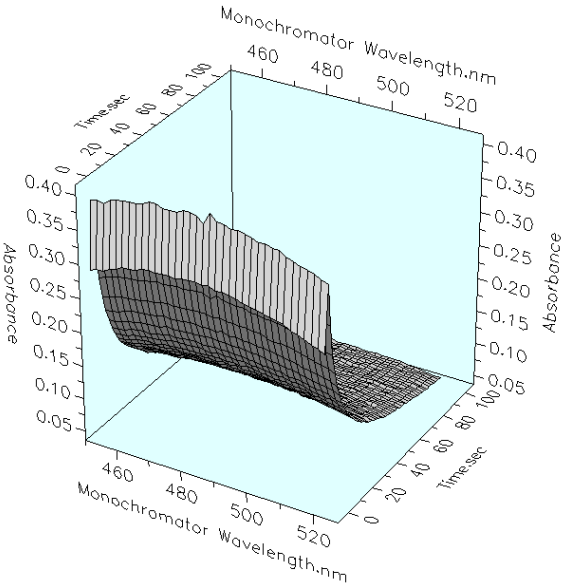

Fig 5: Three-Dimensional plot for reduction of Iron-BHA complex over time.

Furthermore, various results showed that the reduction of Fe(III)-BHA complex was actually a biphasic reaction i.e. a two-step reaction. The kinetics for the both steps were thoroughly studied by varying pH at different concentrations of Hydroxylamine hydrochloride and Fe(III)-BHA complex. Furthermore, the thermodynamic parameters were calculated for both steps. To study the thermodynamic parameters, Eyring equation and Arrhenius equations were used.

Eyring Equation

Equation 1. Calculation of ΔH by Slope of Eyring plot using Eyring equation

$$m\times R=\Delta H$$

In Equation 1, the ideal gas constant (8.3144598 J K^{-1} mol^{-1}) is represented by R, value of

slope is represented by m and is obtained from the graph and the enthalpy change is denoted by ΔH.

The change in entropy was also calculated using the following Eyring plot and the formula to calculate change in entropy (ΔS) was:

Equation 2. Calculation of ΔS from Intercept using Eyring Plot from Eyring Equation.

$$\text{Intercerpt} = \ln\left(\frac{k'}{h}\right) + \frac{\Delta S}{R}$$

$$\Delta S = \left(\text{Intercept} - \ln\left(\frac{k'}{h}\right)\right) \times R$$

In equation 2, the Boltzmann constant (1.380649×10^{-23} J K^{-1}) is given by k', h represents the Plank's constant ($6.62607015 \times 10^{-34}$ Js), R refers to the ideal gas constant (8.3144598 J K^{-1} mol^{-1}), and the change in entropy is shown by ΔS.

Arrhenius equation

Equation 3. Arrhenius Equation

$$\ln k = -\left(\frac{E_A}{RT}\right) + \ln A$$

Arrhenius equation was used to create Arrhenius plots which were used to calculate the energy of activation for the reaction. Using the slope of the plot, activation energy was calculated.

Phase 1:

When studying the Rate of reaction at pH 3.0±0.1 and 3.5±0.1, the concentration of Fe(III)-BHA complex was 1.997×10^{-4} M, the lambda max was set to be 486 nm as discussed before. While, the ionic strength (μ) was 0.2 M. It was noticed that with the increase in concentration of reducing agent NH_3OH^+ Hydroxylamine hydrochloride, the rate of reaction increased. This is because as the amount of catalyst increases, the number of active sites increases as well. This results in more molecules of the Fe(III)-BHA complex being reduced simultaneously. Hence, while the limiting factor is the concentration of reducing agent, increase in hydroxylamine hydrochloride will result in an increase in the rate of reaction however, once the concentration of Fe(III)-BHA complex becomes the limiting factor, i.e. the molecules of Fe(III)-BHA are less in comparison to the molecules of reducing agent, in such case no increase in the rate of reaction will be observed. This increase in the rate can easily be observed in Fig 6(a) and 6(b).

It can also be observed that as temperature is increasing the rate of reaction is also increasing. The following data indicates that the reaction occurring here is an endothermic reaction and as the temperature is being varied from 5±0.5 ºC to 25±0.5 ºC, the rate of reaction is increasing dramatically. The same trend can be observed for pH 4.0±0.1 and 4.5±0.1 as well. Fig 6(a), 6(b), 6(c) and 6(d) all shows that increase in temperature results in increase in rate constant.

In case of pH 4.0±0.1 and 4.5±0.1, the concentration of Fe(III)-BHA complex was 5.0×10^{-5} M. The ionic strength was 0.2 M and the lambda max was the same i.e., 486 nm. It can be seen in Fig 6(c) and 6(d) that the plots are following a similar pattern and with the increase in concentration of reducing agent, the rate constant is increasing. However, this increase is not as significant as the one observed in 6(a) and 6(b). The reason has already been discussed before. This is because this time the concentration of Fe(III)-BHA molecules has been reduced and there is not a high number of complex molecules present in contrast to the reducing agent. Hence, even when there is an increase, it is not as sharp as the one at pH 3.0 and 3.5 where the concentration of Fe(III)-BHA complex was higher.

Regression analysis was used to calculate the thermodynamic parameters including change in enthalpy and change in entropy using the Eyring plots. The plots were formed for different pH. For the analysis, the ionic strength was set to be 0.1 M. For pH 3 and 3.5, the concentration of Fe(III)-BHA complex was set to be 1.997×10^{-4} M while at pH 4 and 4.5 the concentration of the complex was 5.0×10^{-5} M. The same conditions were also set at which the Arrhenius plots were produced.

The Eyring plot Phase I of the reaction, for different pH can be observed in Fig 7. The change in enthalpy and change in entropy at different pH calculated can be observed in Table 2. While the diagrammatical representation of the ΔH and ΔS with their standard deviation can be observed in Fig 9(a) and 9(b).

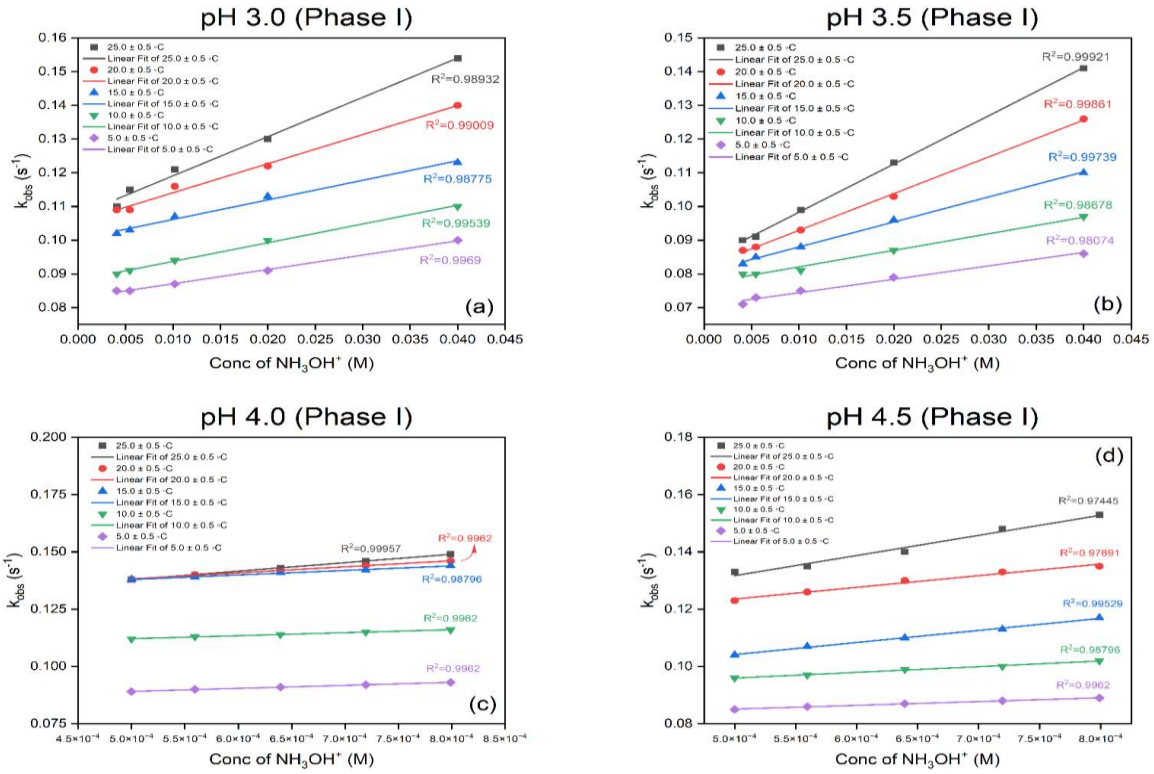

Fig. 6: Rate constant dependance on Hydroxylamine Hydrochloride concentration for Phase I at pH: (a) 3.0±0.1; (b) 3.5±0.1; (c) 4.0±0.1; (d) 4.5±0.1.

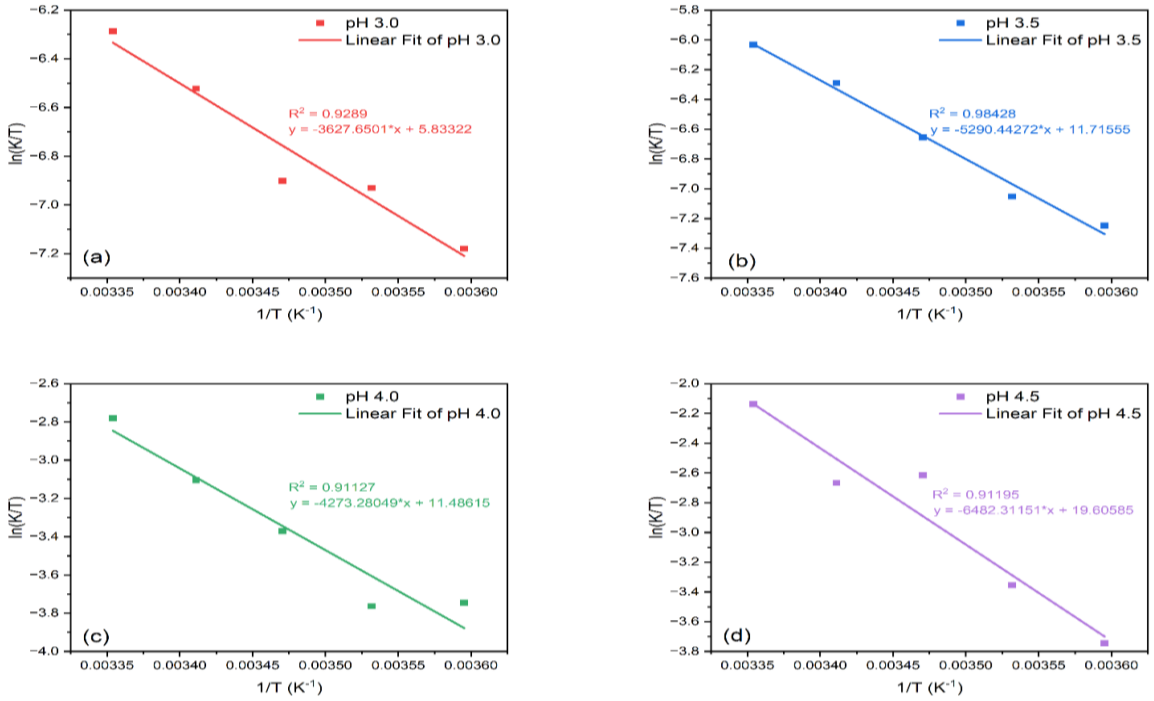

Fig. 7: Eyring plot for Phase I: (a) pH 3; (b) pH 3.5; (c) pH 4.0; (d) pH 4.5.

The Arrhenius plot for phase I against different pH is can be observed in Fig 8. Using these plots and regression analysis, slope was calculated through which activation energy was calculated. The activation energy for phase I at different pH can be observed in table 2 and the diagrammatical representation of activation energy along with its standard deviation can be seen in Fig 9(c).

Table-2: Change in Enthalpy (ΔH), Change in entropy (ΔS) and Activation Energy (Ea) with standard deviation derived from Eyring and Arrhenius Plots for Phase I.

pH	ΔH (kJ mol^{-1})	ΔS (J mol^{-1}K^{-1})	Ea (kJ mol^{-1})
3	30.16 ± 4.17	-149.05 ± 9.58	32.56 ± 4.17
3.5	43.99 ± 1.66	-100.14 ± 8.70	46.38 ± 3.09
4	35.53 ± 6.00	-102.05 ± 4.23	37.92 ± 5.98.
4.5	53.90 ± 8.15	-34.54 ± 5.43	56.29 ± 8.13

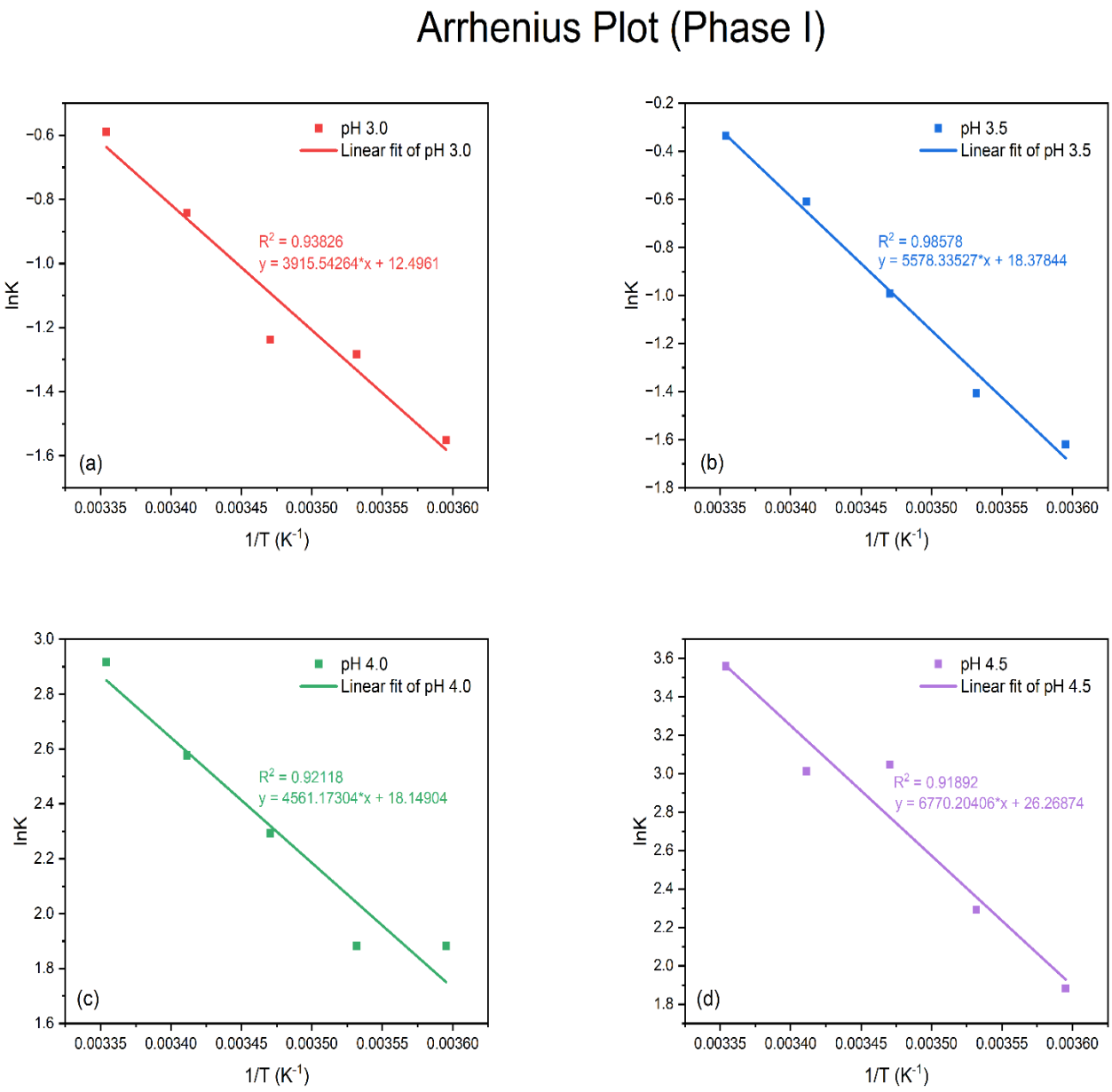

Fig. 8: Arrhenius plot for Phase I: (a) pH 3; (b) pH 3.5; (c) pH 4.0; (d) pH 4.5.

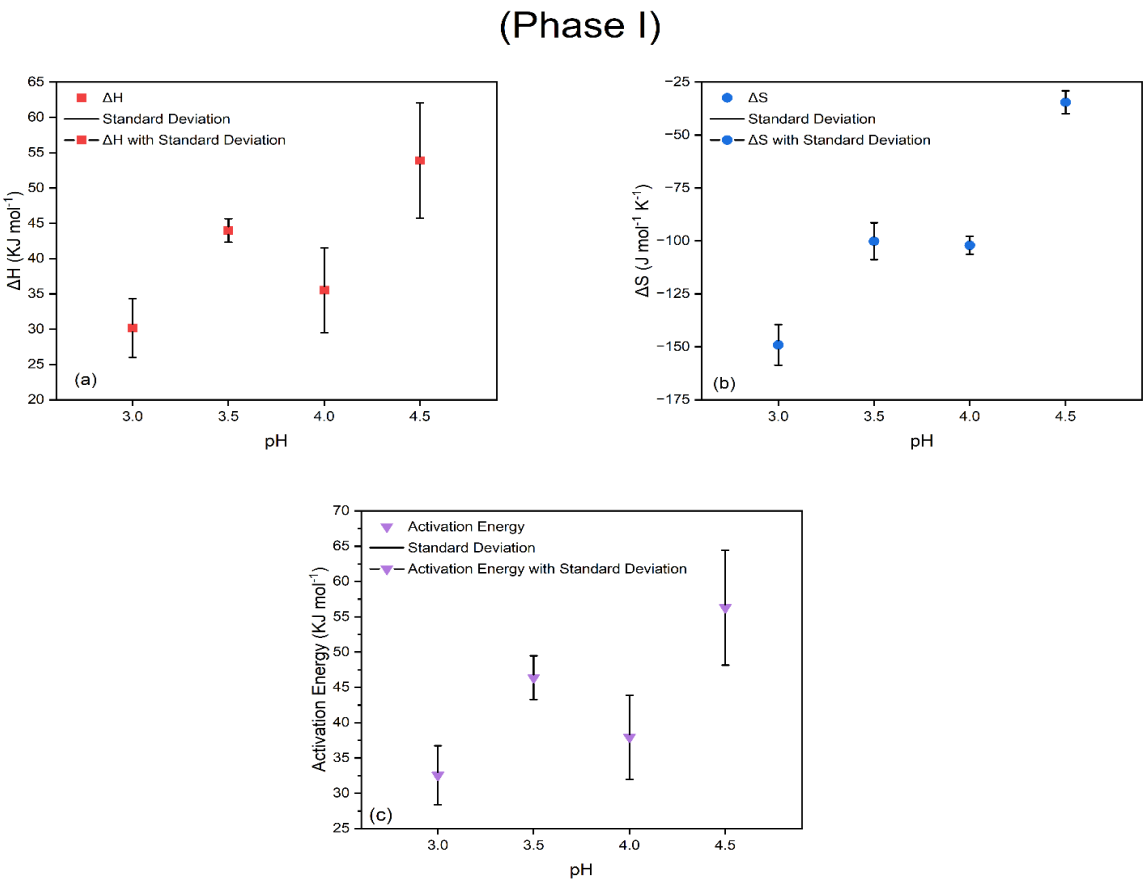

Fig. 9: Thermodynamic Parameters with standard deviation for Phase I: (a) ΔH, (b) ΔS and (c) Activation Energy.

The same parameters were set for analysis of the dependance of rate constant on concentration of the reducing agent and the temperatures ranging from 5±0.5 ˚C to 25±0.5 ˚C. At pH 3.0±0.1 and 3.5±0.1, the concentration of Fe(III)-BHA was set to be 1.997×10^{-4} M while at pH 4.0±0.1 and 4.5±0.1, the Fe(III)-BHA concentration was 5.0×10^{-5} M. The ionic strength was maintained at 0.2 M. The reaction was studied at wavelength of 486 nm. A similar pattern much like in Phase I was seen here as well. The dependance of rate constant on temperature and concentration of reducing agent can be observed in Fig 10.

Phase II

The Eyring plot was also formed in the same manner. The Fig 11 represents the Eyring plots for Phase II at different pH. As done previously, these plots were used to calculate the thermodynamic parameters of change in enthalpy and change in entropy which are given in Table 4. The ΔH and ΔS are also shown graphically with their standard deviation in Fig 13(a) and 13(b).

Table-3: 2nd Order rate constant (k_3) value for specific temperature against a specific pH for Phase I; [Fe(III)-BHA] is set to be 1.997×10^{-4} M, μ at 0.1 M (KCl)

S. No.	pH	T (K)	k_2 (M^{-1} s^{-1})
		298	0.5550
		293	0.4310
1	3.0	288	0.2900
		283	0.2770
		278	0.2120
		298	0.7150
		293	0.5440
2	3.5	288	0.3710
		283	0.2450
		278	0.1980
		298	18.4800
		293	13.1500
3	4.0	288	9.8980
		283	6.5740
		278	6.5740
		298	35.1600
		293	20.3400
4	4.5	288	21.0700
		283	9.8980
		278	6.5740

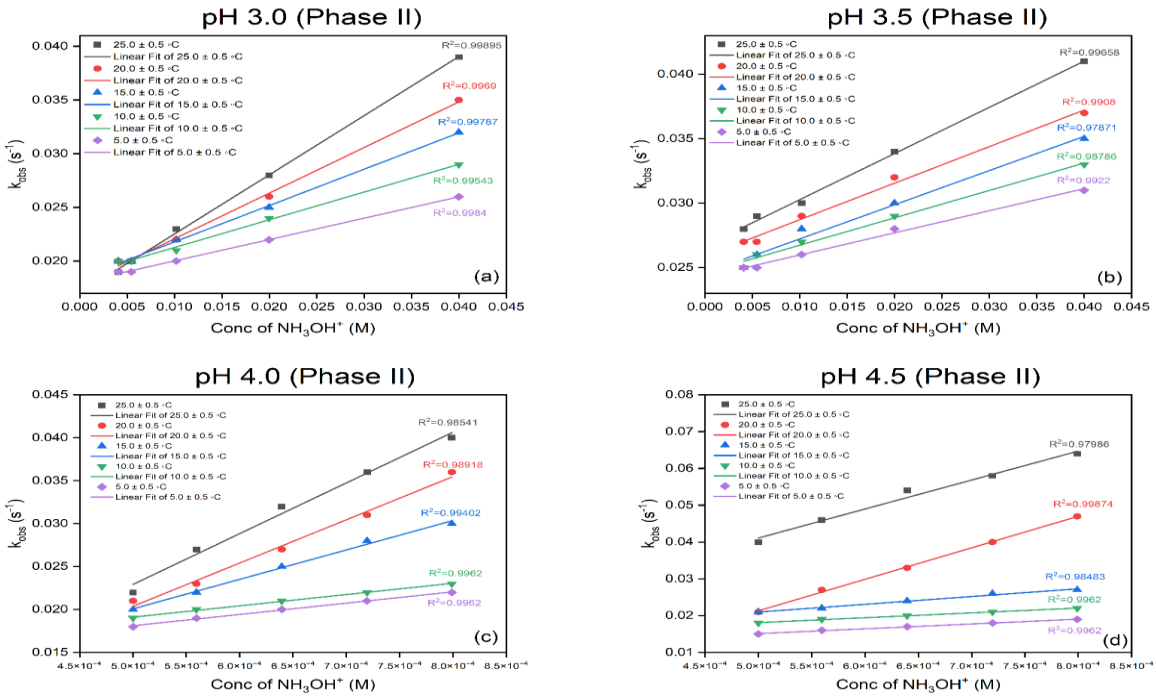

Fig. 10: Rate constant dependance on Hydroxylamine Hydrochloride concentration for Phase II at pH: (a) 3.0±0.1; (b) 3.5±0.1; (c) 4.0±0.1; (d) 4.5±0.1.

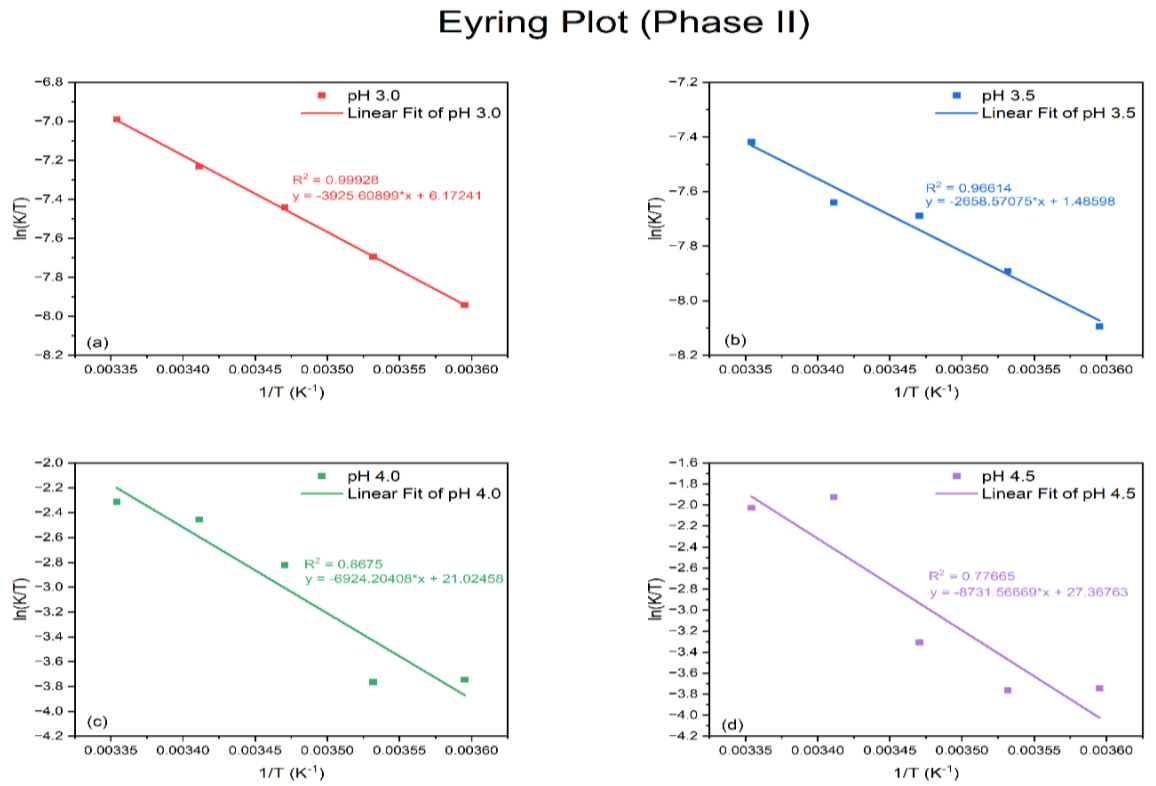

Fig. 11: Eyring plot for Phase II: (a) pH 3; (b) pH 3.5; (c) pH 4.0; (d) pH 4.5.

The Arrhenius plots for Phase II can be observed in Fig 12. The calculation of slope was used to calculate activation energy which has been reported in Table 4. The graphical representation of activation energy at different pH for phase II can also be observed in Fig 13(c) along its standard deviation.

Table-4: Thermodynamic Parameters with standard deviation for Phase II: (a) ΔH; (b) ΔS and (c) Activation Energy

pH	ΔH (kJ mol^{-1})	ΔS (J mol^{-1} K^{-1})	Ea (kJ mol^{-1})
3	32.64 ± 1.67	-146.23 ± 0.18	35.03 ± 1.86
3.5	22.10 ± 2.34	-185.20 ± 0.91	24.50 ± 2.28
4	57.57 ± 9.39	-22.74 ± 15.56	59.96 ± 9.39
4.5	72.60 ± 6.20	29.99 ± 19.21	74.99 ± 12.22

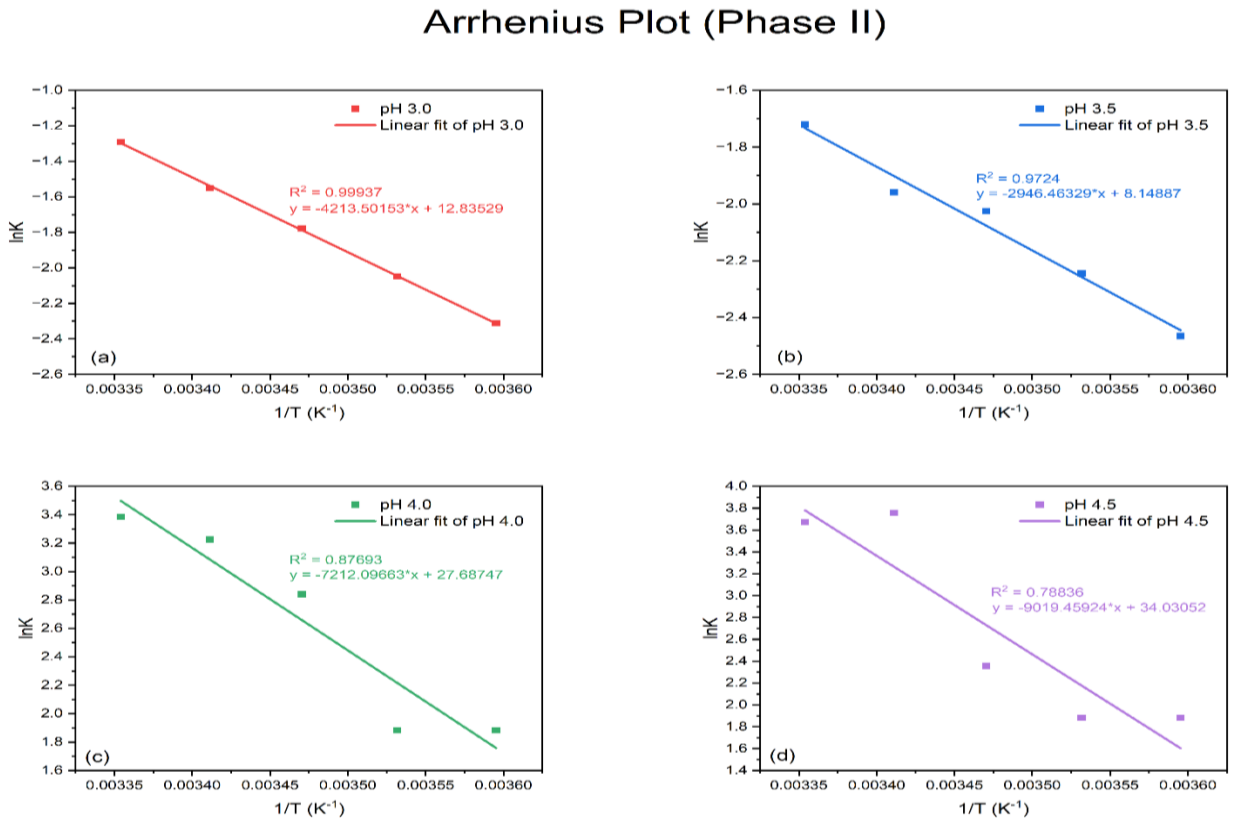

Fig. 12: Arrhenius plot for Phase II: (a) pH 3; (b) pH 3.5; (c) pH 4.0; (d) pH 4.5.

Table-5: 2nd Order rate constant (k_4) value for specific temperature against a specific pH for Phase II; [Fe(III)-BHA] is set to be 1.997×10^{-4} M, μ at 0.1 M (KCl).

S. No.	pH	T (K)	k_2 (M^{-1} s^{-1})
		298	0.2750
		293	0.2120
1	3.0	288	0.1690
		283	0.1290
		278	0.0990
		298	0.1790
		293	0.1410
2	3.5	288	0.1320
		283	0.1060
		278	0.0850
		298	29.5100
		293	25.1600
3	4.0	288	17.1300
		283	6.5740
		278	6.5740
		298	39.3700
		293	42.8000
4	4.5	288	10.5500
		283	6.5740
		278	6.5740

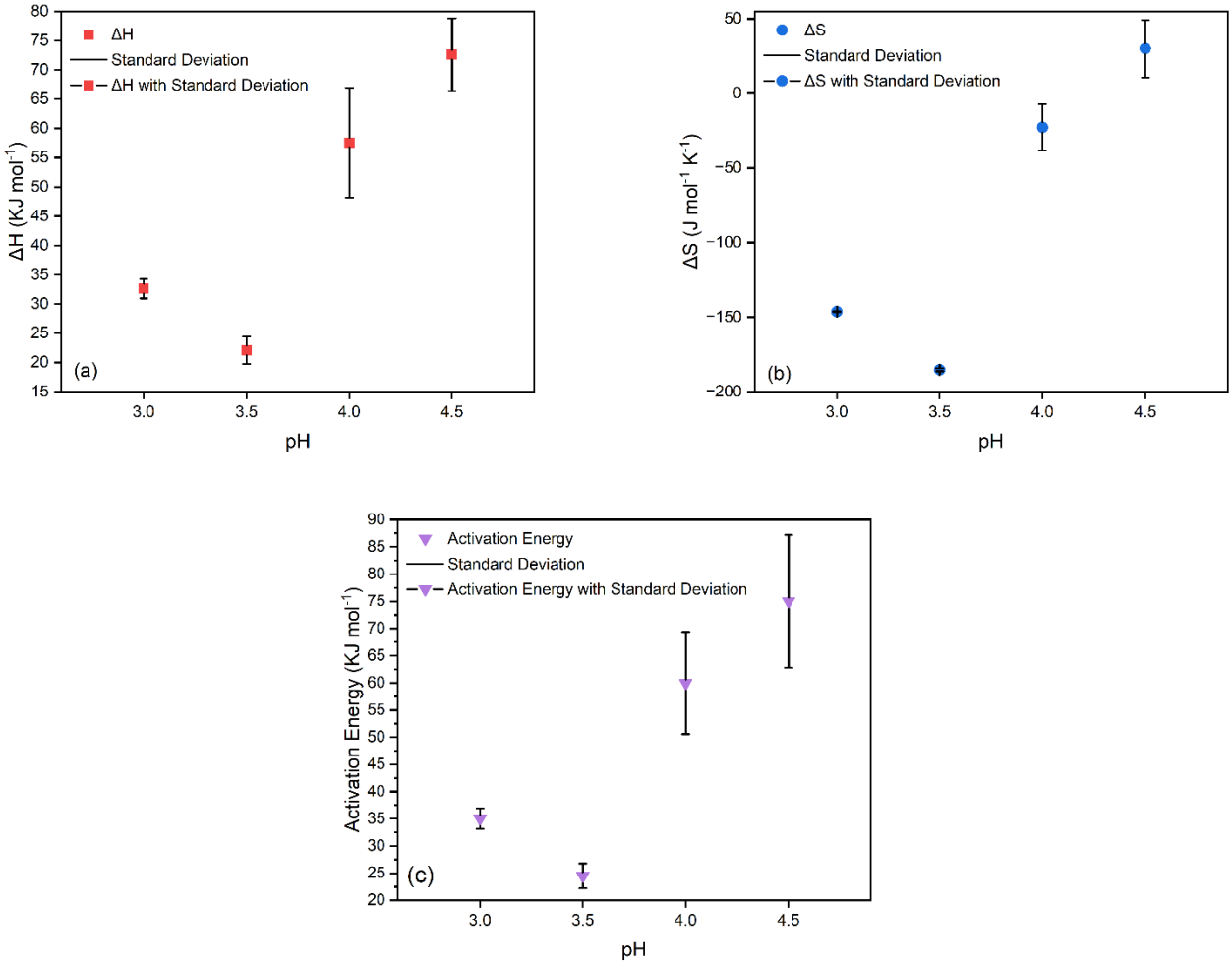

Fig. 13: Thermodynamic Parameters with standard deviation for Phase II: (a) ΔH; (b) ΔS and (c) Activation Energy.

Iron-BHA Complex Reduction Mechanism with Hydroxylamine hydrochloride

Under the experimental conditions, we proposed the following mechanism;

Fast Phase

$$H^+ + Fe^{3+}(BHA)_3 \underset{k_{-1}}{\overset{k_1}{\rightleftharpoons}} Fe^{+3}(BHA)_2 + HBHA$$

The above equilibrium exists at low pH.

$$Fe^{+3}(BHA)_2 + NH_3OH^+ \xrightarrow{k_2} Fe^{+2} + 2BHA^- + NH_2OH^+ + H^+$$

Applying steady-state approximation (SSA);

$$\frac{dFe^{+3}(BHA)_2}{dt} = -\frac{dFe^{+3}(BHA)_2}{dt}$$

$$\text{Rate of appearance} = \frac{d\left[Fe^{III}(BHA)_2\right]}{dt} = k_1\left[Fe^{III}(BHA)_3\right]\left[H^+\right]$$

$$\text{Rate of disappearance} = -\frac{d\left[Fe^{III}(BHA)_2\right]}{dt} = k_{-1}\left[Fe^{III}(BHA)_2\right]\left[HBHA\right] + k_2\left[Fe^{III}(BHA)_2\right]\left[NH_3OH^+\right]$$

Under steady-state conditions;

Rate of appearance = Rate of disappearance

$$k_1\left[Fe^{III}(BHA)_3\right]\left[H^+\right] = k_{-1}\left[Fe^{III}(BHA)_2\right]\left[HBHA\right] + k_2\left[Fe^{III}(BHA)_2\right]\left[NH_3OH^+\right]$$

$$\left[Fe^{III}(BHA)_2\right]\left(k_{-1}\left[HBHA\right] + k_2\left[NH_3OH^+\right]\right) = k_1\left[Fe^{III}(BHA)_3\right]\left[H^+\right]$$

$$\left[Fe^{III}(BHA)_2\right]=\frac{k_1\left[Fe^{III}(BHA)_3\right]\left[H^+\right]}{\left(k_{-1}\left[HBHA\right]+k_2\left[NH_3OH^+\right]\right)}$$

We know that $[H^+] = \text{constant}$; $k_1[H^+] = k_3$

$$\text{Rate}=\frac{k_2k_1\left[Fe^{III}(BHA)_3\right]\left[H^+\right].\left[NH_3OH^+\right]}{\left(k_{-1}\left[HBHA\right]+k_2\left[NH_3OH^+\right]\right)}$$

$$k_{obs}=\frac{k_2.k_3\left[NH_3OH^+\right]}{\left(k_{-1}\left[HBHA\right]+k_2\left[NH_3OH^+\right]\right)}$$

If $k_{-1}\left[HBHA\right]>>k_2\left[NH_3OH^+\right]$ so, it can be neglected.

Thus, $k_{obs}=\frac{k_2.k_3\left[NH_3OH^+\right]}{k_{-1}\left[HBHA\right]}$

The rate constant is directly proportional to the $[NH_3OH^+]$.

But, if $k_2\left[NH_3OH^+\right]>>k_{-1}\left[HBHA\right]$ then, it can be neglected, $k_{obs}=k_3$ i.e., $k_3=k_1\left[H^+\right]$

$$k_{obs}=\frac{k_2.k_3\left[NH_3OH^+\right]}{k_2\left[NH_3OH^+\right]}$$

$$k_{obs}=k_3$$

and

$$k_3=k_1\left[H^+\right]$$

During the oxidation of $NH_3OH^+$the changes can be brought about, are as follows:

$$Fe^{+3} + NH_3OH^+ \longrightarrow Fe^{+2} + NH_2OH^+ + H^+$$

$$Fe^{+3} + NH_2OH^+ \longrightarrow Fe^{+2} + NHO\cdot + 2H^+$$

$$2NHO\cdot \longrightarrow H_2N_2O_2$$

So, the overall reaction is;

$$4Fe^{+3} + 2NH_3OH^+ \longrightarrow 4Fe^{+2} + H_2N_2O_2 + 6H^+$$

Slow Phase

The plausible mechanism for the slow phase of reduction of Fe^{III}-BHA by NH_3OH^+:

$$[Fe^{III}(BHA)_3] + [NH_3OH^+] \xrightarrow{k_4} [Fe^{II}(BHA)_3]$$

Rate Law can be written as

$$\left[Fe^{III}(BHA)_3\right]=\left[Fe^{III}(BHA)_3\right]\left[NH_3OH^+\right]$$

$$-\frac{d\left[Fe^{III}(BHA)_3\right]}{dt}=k_4\left[Fe^{III}(BHA)_3\right]\left[NH_3OH^+\right]$$

$k_{obs}=k_4\left[NH_3OH^+\right]$, it clearly shows the rate constant is depending upon the concentration of hydroxylamine hydrochloride.

$$\text{Rate}=-\frac{d\left[Fe^{III}(BHA)_3\right]}{dt}=k_{obs}\left[Fe^{III}(BHA)_3\right]$$

Conclusion

To avoid Iron undergoing Fenton Reaction and for making Iron available to different living organisms, it can be observed that Siderophores usage is extremely important. However, for the removal of Iron from such siderophores, processes like reduction are to be employed. Iron-BHA has been very successfully reduced with the help of Hydroxylamine Hydrochloride, emerging as a viable reductant. The reduction process comprised of two steps and both of the steps were dependent on pH and temperature. In both the Phases (Step 1 and 2) it was noticed that the reaction rate increased with the increase in temperature from 278 K to 298 K. Similarly, a spike in rate constant was also observed by increasing the concentration of Hydroxylamine hydrochloride, this increase was significant but relatively smaller than the change caused by temperature. The thermodynamic parameters like Change in Enthalpy, Entropy and Activation energy for both steps were calculated. For Phase 1, at pH 3, 3.5, 4 and 4.5, the change in enthalpy was 30.16±4.17, 43.99±1.66, 35.53±6.00 and 53.90±8.15 kJ mol^{-1} respectively. Change in entropy was -149.05±9.58, -100.14±8.70, -102.05±4.23 and -34.54±5.43 J mol^{-1} K^{-1} while the activation energy was 32.56±4.17, 46.38±3.09, 37.92±5.98 and 56.29±8.13 kJ mol^{-1} respectively. For step 2, at pH 3, 3.5, 4 and 4.5, the change in enthalpy was reported to be 32.64±1.67, 22.10±2.34, 57.57±9.39 and 72.60±6.20 kJ mol^{-1} respectively. Activation energy was 35.03±1.86, 24.50±2.28, 59.96±9.39 and 74.99±12.22 kJ mol^{-1} and change in entropy was -146.23±0.18, -185.20±0.91, -22.74±15.56 and 29.99±19.21 J mol^{-1} K^{-1} respectively. Therefore, for the bioavailability of Iron, hydroxylamine hydrochloride being used as a reducing agent has unveiled newer pathways in the world of nutrients.

Acknowledgement

I am grateful to my beloved mentor and Eminent Scientist, Prof. Dr. Arif Kazmi, HEJ, Research Institute of Chemistry, University of Karachi, Karachi-75270, for his step-by-step expert opinions and guidance.

References

1. S.J. Lippard, J.M. Berg, Principles of bioinorganic chemistry, University Science Books, (1994).
2. J. Neilands, A brief history of iron metabolism, Biology of metals, 1-6 (1991).
3. D. Touati, Iron and oxidative stress in bacteria, Archives of biochemistry and biophysics., **373(1)**, 1-6 (2000).
4. H. Budzikiewicz, Bacterial citrate siderophores, Mini-Reviews in Organic Chemistry., **2(2)**, 119-124 (2005).
5. C. Sprencel, Z. Cao, Z. Qi, D.C. Scott, M.A. Montague, N. Ivanoff, J. Xu, K.M. Raymond, S.M. Newton, P.E. Klebba, Binding of ferric enterobactin by the Escherichia coli periplasmic protein FepB, Journal of bacteriology., **182(19)**, 5359-5364 (2000).
6. K. Postle, Active transport by customized β–barrels, Nature structural biology., **6(1)**, 3-6 (1999).
7. J.J. De Voss, K. Rutter, B.G. Schroeder, C.E. Barry III, Iron acquisition and metabolism by mycobacteria, Journal of bacteriology., **181(15)**, 4443-4451 (1999).
8. C. Ratledge, L.G. Dover, Iron metabolism in pathogenic bacteria, Annual reviews in microbiology., **54(1)**, 881-941 (2000).
9. S.C. Andrews, A.K. Robinson, F. Rodríguez-Quiñones, Bacterial iron homeostasis, FEMS microbiology reviews., **27(2-3)**, 215-237 (2003).
10. A.-M. Albrecht-Garyl, Coordination Chemistry of Siderophores: Thermodynamics and Kinetics, Metal ions in biological systems., **309**, 239 (1998).
11. A. Stintzi, C. Barnes, J. Xu, K.N. Raymond, Microbial iron transport via a siderophore shuttle: a membrane ion transport paradigm, Proceedings of the National Academy of Sciences., **97(20)**, 10691-10696 (2000).
12. J. Pierre, M. Fontecave, R. Crichton, Chemistry for an essential biological process: the reduction of ferric iron, Biometals., **15(4)**, 341-346 (2002).
13. K.N. Raymond, E.A. Dertz, S.S. Kim, Enterobactin: an archetype for microbial iron transport, Proceedings of the national academy of sciences., **100(7)**, 3584-3588 (2003).
14. S. Dhungana, A.L. Crumbliss, Coordination chemistry and redox processes in siderophore-mediated iron transport, Geomicrobiology Journal., **22(3-4)**, 87-98 (2005).
15. M. Sandy, A. Butler, Microbial iron acquisition: marine and terrestrial siderophores, Chemical reviews., **109(10)**, 4580-4595 (2009).
16. I. Jilal, S. El Barkany, Z. Bahari, O. Sundman, A. El Idrissi, M. Abou-Salama, A. Romane, C. Zannagui, H. Amhamdi, New quaternized cellulose based on hydroxyethyl cellulose (HEC) grafted EDTA: Synthesis, characterization and application for Pb (II) and Cu (II) removal, Carbohydrate polymers., **180**, 156-167 (2018).
17. C. Bradbeer, The proton motive force drives the outer membrane transport of cobalamin in Escherichia coli, Journal of bacteriology., **175(10)**, 3146-3150 (1993).
18. J.M. Harrington, A.L. Crumbliss, The redox hypothesis in siderophore-mediated iron uptake, Biometals., **22(4)**, 679-689 (2009).
19. H. Boukhalfa, A.L. Crumbliss, Chemical aspects of siderophore mediated iron transport, Biometals., **15(4)**, 325-339 (2002).
20. R.E. Moore, Y. Kim, C.C. Philpott, The mechanism of ferrichrome transport through Arn1p and its metabolism in Saccharomyces cerevisiae, Proceedings of the National Academy of Sciences., **100(10)**, 5664-5669 (2003).
21. I. Spasojević, S.K. Armstrong, T.J. Brickman, A.L. Crumbliss, Inorg. Chem., **38**, 449-454 (1999).
22. A. MOHAMED AZIZI Bassair, F.Z. LAKHDAR, PGPR: outils microbiologiques potentiellement promotrices de la croissance des plantes aux vertus médicinales, cas de Cresson (Lepidium sativum), (2022).
23. D.H. Howard, Acquisition, transport, and storage of iron by pathogenic fungi, Clinical microbiology reviews., **12(3)**, 394-404 (1999).
24. H. Beinert, R.H. Holm, E. Munck, Iron-sulfur clusters: nature's modular, multipurpose structures, Science,. **277(5326)**, 653-659 (1997).
25. A.L. Crumbliss, J.M. Harrington, Iron sequestration by small molecules: thermodynamic and kinetic studies of natural siderophores and synthetic model compounds, Advances in inorganic chemistry., **61**, 179-250 (2009).
26. S.R. Cooper, J.V. McArdle, K.N. Raymond, Siderophore electrochemistry: relation to intracellular iron release mechanism, Proceedings of the National Academy of Sciences., **75(8)**, 3551-3554 (1978).
27. M.Y. Kwak, J.S. Rhee, Cultivation characteristics of immobilized Aspergillus oryzae for kojic acid

production, Biotechnology and bioengineering., **39(9)**, 903-906 (1992).
28. H. Boukhalfa, T.J. Brickman, S.K. Armstrong, A.L. Crumbliss, Kinetics and mechanism of iron (III) dissociation from the dihydroxamate siderophores alcaligin and rhodotorulic acid, Inorganic Chemistry., **39(25)**, 5591-5602 (2000).
29. J. Neilands, A crystalline organo-iron pigment from a rust fungus (Ustilago sphaerogena), Journal of the American Chemical Society., **74(19)**, 4846-4847 (1952).
30. B. Monzyk, A.L. Crumbliss, Mechanism of ligand substitution on high-spin iron (III) by hydroxamic acid chelators. Thermodynamic and kinetic studies on the formation and dissociation of a series of monohydroxamatoiron (III) complexes, Journal of the American Chemical Society., **101(21)**, 6203-6213 (1979).
31. F. Hallé, J.M. MEYER, Iron release from ferrisiderophores: A multi-step mechanism involving a NADH/FMN oxidoreductase and a chemical reduction by FMNH2, European journal of biochemistry., **209(2)**, 621-627 (1992).
32. B.F. Matzanke, S. Anemüller, V. Schünemann, A.X. Trautwein, K. Hantke, Fhuf, part of a siderophore− reductase system, Biochemistry., **43(5)**, 1386-1392 (2004) .
33. M. Hassan, S. Nisar, S. Kazmi, M. Qadri, S. Imad, R. Naz, Kinetics and Mechanism of Reduction of Fe (III)-Acetohydroxamic Acid by Hydroxylamine Hydrochloride at Acidic pH, Pakistan Journal of Chemistry., **5(1)** (2015).